

Large-Area Triboelectric Nanogenerator Mass Spectrometry: Expanded Coverage, Double-Bond Pinpointing, and Supercharging

Marcos Bouza, Yafeng Li, Changsheng Wu, Hengyu Guo, Zhong L. Wang, and Facundo M. Fernández*


 Cite This: <https://dx.doi.org/10.1021/jasms.0c00002>


Read Online

ACCESS |



Metrics & More

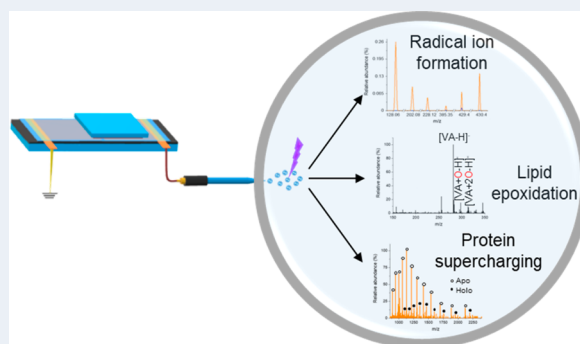


Article Recommendations



Supporting Information

ABSTRACT: Efficient ionization is a necessary condition for mass spectrometric analysis, but many compounds fail to ionize well enough to yield sufficient detection limits. Triboelectric nanogenerators (TENG) coupled to nanoelectrospray ionization (nanoESI) mass spectrometry (MS) are a highly effective approach to high sensitivity MS analysis. Here, we report on new, large-area TENG that constructively leverage the relationship between electrode size, created charges, and open-circuit voltage, leading to wider chemical coverage. Large-area TENG were found to also promote electrospray gas-phase oxidation reactions that enabled double bond position pinpointing for unsaturated lipids and species-specific lipid quantitation. Furthermore, large-area TENG MS of proteins was observed to yield higher charge state distributions (i.e., supercharging) without the need for high surface tension additives.



The pioneering experiments of Yamashita and Fenn published in 1984¹ first suggested the role that electrospray ionization (ESI) coupled to mass spectrometry (MS) would later have as a powerful characterization tool. Nowadays, both ESI and nanoESI MS² have matured as part of essential bioanalytical platforms and are central to fields such as metabolomics and proteomics.^{3,4} Continuous research efforts directed at improving ESI and its open air “ambient” counterparts such as desorption electrospray ionization (DESI) and nanoDESI^{5–7} have led to increased sample throughput, better tolerance to complex matrices, and extended chemical coverage.^{8–10}

Typically, ESI, DESI, and even ion sources for imaging MS such as laser ablation electrospray ionization (LAESI)¹¹ are powered by high voltage DC supplies. As an alternative, both static electricity^{12,13} and triboluminescence^{14,15} have been proposed as simpler, gentler, and safer alternatives for driving MS ionization. Demonstrated advantages of these new approaches include added simplicity, ion kinetic energies that preserve noncovalent complex structures,¹² and improved sensitivity for both peptides and proteins.¹³

Triboelectric nanogenerators (TENG), first introduced by Wang et al. as mechanic motion-harnessing devices to power electronics, are one of the most effective means of static electricity utilization.^{16–19} In TENG, different dielectric materials and designs are used to generate electricity based on triboelectrification and electrostatic induction.²⁰ TENG are capable of producing hundreds of $\mu\text{C m}^{-2}$ per cycle and open-circuit voltages in the several kilovolt range, with proved stability of up to millions of cycles with minimal degradation.²¹

Our team recently described the first use of contact separation (CS) and sliding freestanding (SF)-TENG as nanoESI power sources,²² and their application to the analysis of counterfeit medicines.²³ Among the tested configurations, SF-TENG showed excellent sensitivity and reproducibility, with much improved detection limits.

One of the special characteristics of TENG is that their open-circuit voltages and amount of charges generated per cycle are based on the choice of electrode materials and size, so larger area TENG produce higher amounts of delivered charges to the ion source, potentially resulting in unexplored analytical advantages. In this work, a large-area TENG-driven nanoESI ion source is characterized in terms of the polarity range of ionizable metabolites, gas-phase reactions at the emitter tip, droplet size distributions, and extent of analyte charging. Results indicate significant improvements for difficult-to-ionize analytes, the noteworthy capability to enable rapid double bond pinpointing in unsaturated lipids, and the ability to induce protein supercharging without additives.

EXPERIMENTAL METHODS

Materials and Chemicals. Optima LC–MS grade acetonitrile (ACN), acetone, 2-propanol, methanol (MeOH),

Received: January 7, 2020

Revised: January 14, 2020

Accepted: January 15, 2020



and chloroform (CHCl_3) (Fisher Chemical, Suwanee, GA) and ultrapure 18.2 M Ω -cm deionized water (Barnstead Nanopure Diamond, Van Nuys, CA) were used for preparing all solutions. Human serum was purchased from Sigma-Aldrich (Saint Louis, MO). Fatty acid (FA) extraction from such sample was performed using a HybridSPE-phospholipid removal cartridge (30 mg, Sigma-Aldrich, Saint Louis, MO), followed by liquid/liquid extraction with chloroform:methanol; a detailed extraction procedure is provided in the [Supporting Information](#). Ammonium hydroxide (NH_4OH) (20–30%), trifluoroacetic acid (TFA), ammonium acetate (NH_4Ac), and ammonium bicarbonate (NH_4Bic) were purchased from Fisher Chemical (Suwanee, GA). Inosine, pyrene, cholesterol, α -tocopherol, naphthalene, bisphenol A, oleic acid, *cis*-vaccenic acid, linoleic acid, α -linolenic acid, heptadecanoic acid, sucrose, cytochrome c from bovine heart, myoglobin from equine skeletal muscle, and ubiquitin from bovine red blood cells were purchased from Sigma-Aldrich (Saint Louis, MO).

TENG-MS. Experiments were carried out using a manually actuated large-area SF-TENG that powered a nanoESI ion source coupled to a Q-Exactive hybrid quadrupole-Orbitrap mass spectrometer (Thermo Scientific, San Jose, CA). For DC nanoESI experiments, the spectrometer's own power supply was used, with a voltage of 1.5 kV. Glass emitter tips (Econo 12, New Objective, i.d. = 0.69 mm, o.d. = 1.2 mm, part no. ECONO 12N) were employed in all cases. The nanoESI emitters were mounted on an *x*, *y*, *z* manual linear stage (Thorlabs, Newton, NJ) to control position with respect to the mass spectrometer capillary inlet; unless specified otherwise, the emitter tip was held 8–10 mm away from the capillary inlet. A 1.5 mm diameter silver wire was inserted into the emitters to provide electric contact with the sample solution.

The following instrumental conditions were used for Q-Exactive MS experiments unless specified otherwise: capillary temperature: 150 °C, S-lens radio frequency level: 50, maximum injection time: 50 ms, automatic gain control: 5×10^6 , mass resolution: 17500 for small molecules and 70000 for protein analysis. For tandem MS experiments, a resolving power of 17500 and fragmentation energy of 35 NCE units were used.

The large-area SF-TENG consisted of two static electrodes (Cu film deposited onto FEP as two rectangles separated by an uncoated rectangular region, mounted on acrylic) of 135 and 121 cm², and a movable slider (Nylon mounted onto a foam square supported by an acrylic piece) of 127 cm². In all cases, TENG were actuated manually for mechanistic studies, as sufficient reproducibility was obtained without the need for electrical actuators. The smaller movable slider electrode used in some comparative experiments was similar to the one previously used by our group,²² and was built with cooper foil deposited on a 35.75 cm² acrylic piece. A linear motor (LinMot USA, Inc.) or a UR5 robotic arm (Universal Robots, Inc.) was used to operate the movable slider electrode in experiments where automation was implemented.

NanoESI Spray and Emitter Imaging. Electrospray images were collected using a mobile phone camera and a line laser (532 nm, 50 mW, class I, BES532-L, Apinex, Montreal, Canada), positioned at 90° with respect to the nanoESI emitters. The laser was used to illuminate the plume generated at the tip. NanoESI tip emitter images before and after TENG operation were captured using a Hitachi SU8010 ultrahigh resolution scanning electron microscope (SEM). The

aerosol droplet distribution was characterized using a scanning mobility particle sizer spectrometer (SMPS model 3938, TSI, Inc., MN), also known as a differential mobility analyzer (DMA). These experiments were performed using a 1% sucrose solution with 200 mM NH_4Ac added; a detailed explanation of DMA experiments is provided in the [Supporting Information](#).

RESULTS AND DISCUSSION

Large-Area TENG Characterization. Two static electrodes and a movable slider with different triboelectric layers were used to construct the SF-TENG used in this work. Displacement of this slider between the two center positions of the static electrodes alters the electrostatic balance on the dielectric materials, producing a net charge displacement through the nanoESI ion source. The proportionality between the amount of charge generated by TENG and their electrode area, together with the desire for a better understanding of the underlying ionization mechanisms in TENG MS,²² led us to the construction of an SF-TENG with ~2.5-fold larger electrodes compared to our initial devices ([Figure 1a](#)). The

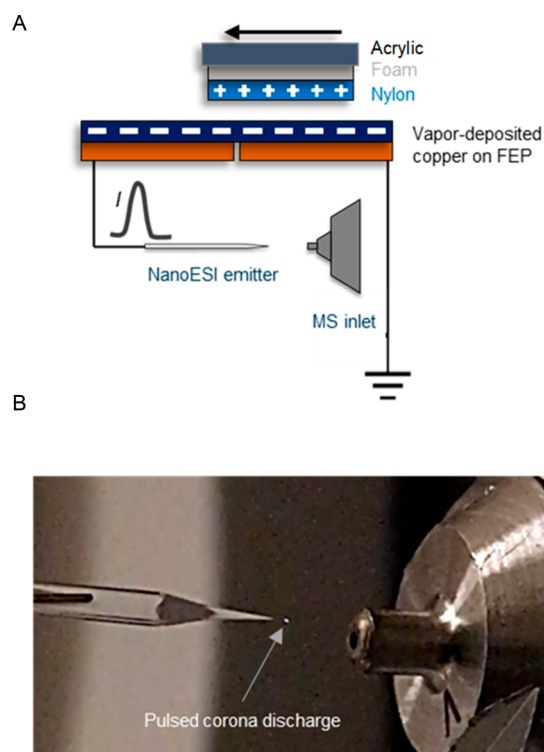


Figure 1. (a) Schematic describing the large-area TENG device. (b) Photography of the pulsed corona discharge observed at the glass emitter tip during the negative voltage operation cycle.

implemented design produced open-circuit voltages of 6–7 and 5.5–6.5 kV and 5 and 7.3 mA of pulse maximum currents in positive- and negative-ion modes, respectively ([Figure S1a,b](#)), values that exceeded those in our previous work.²² Percent relative standard deviations (RSD%) of the generated voltages, current, and total ion chromatogram abundances ([Figure S1c](#)) were 11.6–12.8%, 11.3–14.1%, and 10.7%, respectively. The large majority of mechanistic experiments presented in this work were conducted with manually actuated TENG, but both synchronized and unsynchronized TENG-MS

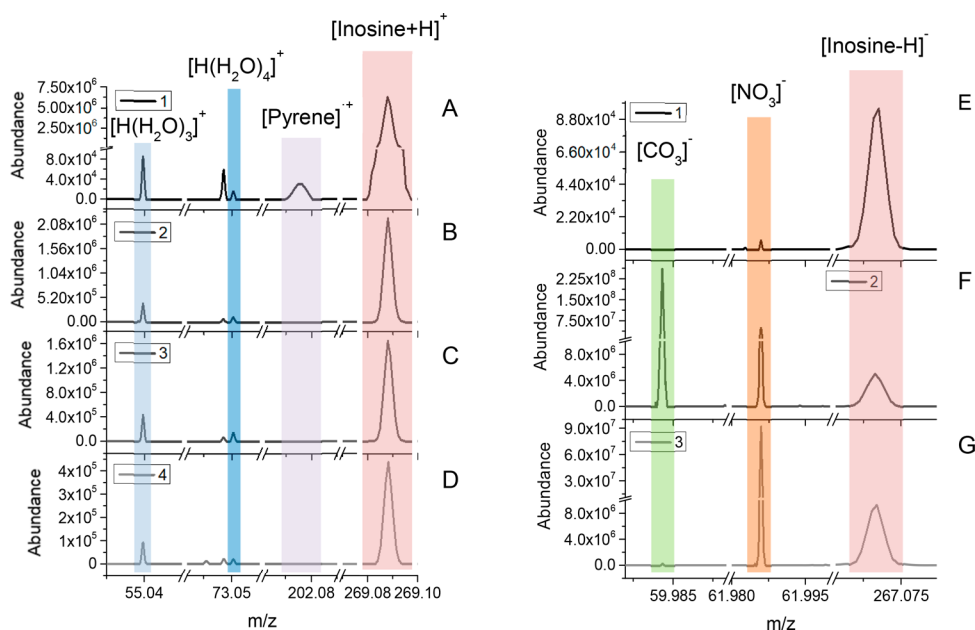


Figure 2. Temporal evolution of the ion signals during a large-area TENG cycle for a 10 μM pyrene and 10 μM inosine (1:1) water/methanol solution with 0.1% TFA in positive-ion mode at different time points described in Figure S3: 1 (a), 2 (b), 3 (c), 4 (d). The same solution in negative-ion mode at different pulse time points: 1 (e), 2 (f), and 3 (g).

analysis can also be performed using mechanical actuators, with examples discussed in Figure S2.

The higher open-circuit voltages achieved by the large-area TENG led to the formation of a transient corona discharge that was only visible to the naked eye during the first ~ 0.1 s of the negative-ion mode operation cycle (Figure 1b), but not during positive-ion mode operation. The absence of observable light emission in positive-ion mode, however, is not indicative of a lack of corona discharge during TENG operation. Both Konermann et al.²⁴ and Morozov et al.²⁵ have shown the formation of reactive oxidized species in discharges not visible by the naked eye. Those electro spray-associated plasmas are typically classified as glow corona discharges,²⁶ with several reports of their stabilizing effect whenever the streamer regime conditions are not reached.^{27,28} Detection of reactant ions typically formed during atmospheric pressure chemical ionization (APCI) also confirmed the presence of a plasma during TENG MS operation. Protonated water clusters, such as $[(\text{H}_2\text{O})_3 + \text{H}]^+$ and $[(\text{H}_2\text{O})_4 + \text{H}]^+$, were detected during the positive portion of the TENG cycle (Figure 2a), with mass accuracies of 1.8 and -0.9 ppm, respectively. In a similar fashion, the negative portion of the cycle led to the formation of reactant ions that included species such as $[\text{CO}_3]^-$ and $[\text{NO}_3]^-$ (Figure 2e–g), known to be of importance in negative-ion mode APCI.²⁹ The temporal evolution of the abundance of such reactant species (Figure 2b–d,f,g), together with the molecular ions of pyrene ($[\text{M}]^+$, m/z 202.078) and inosine ($[\text{M} + \text{H}]^+$, m/z 269.088), was measured at various time points (Figure S3) of the ion transient. It was observed that the APCI-like processes occurring during the corona discharge event promoted pyrene radical ion formation at the maximum of the voltage transients (Figure S1a) and during the current spike observed in the negative portion of the TENG operation cycle (Figure S1b). In positive-ion mode, inosine showed an abundance maximum that coincided with the maximum TENG output voltage, whereas in negative-ion mode (Figure 2b) the abundance increased as the corona

discharge subsided, likely due to a progressive switch from an APCI to an ESI-prevalent regime. The voltages associated with each TENG ion pulse (5.5–7 kV) led to the formation of dual-jet sprays during the positive portion of the cycle (Figure S4). Formation of such multiple jets is considered a step prior to the appearance of corona discharges,³⁰ and therefore reinforced the finding that transient high voltages caused by the larger TENG area caused a corona discharge event. Such corona discharges had an approximate duration of ~ 100 ms at the beginning of each ~ 1 s TENG ion pulse. Scanning electron microscopy images of emitters subject to such discharges showed no appreciable damage to the emitter tip even after 200 TENG operation cycles (Figure S5). The transient nature of the TENG corona discharge seemed to reduce the thermal stress produced by the electrical breakdown, allowing prolonged operation with excellent reproducibility.

To further characterize the effect of the transient high voltages produced during large-area TENG ionization, droplet size distributions were studied using the aerosol created by a 1% sucrose solution as a surrogate (Figure S6), as previously described.^{31–33} For DC nanoESI, measured sucrose particle sizes ranged from 18 to 40 nm, with a significant population of droplet sizes likely missed by DMA measurements in positive-ion mode due to the instrument size cutoff. Increasing spray voltage in negative-ion mode DC nanoESI increased particle sizes (Figure S6c). Large-area TENG yielded larger and more abundant particles than DC nanoESI (Figure S6d), this higher abundance likely being one of the reasons behind the increased sensitivity observed for large-area TENG, as discussed below.

The dual ESI/APCI mechanism responsible for the results in Figure 2 was further investigated using a mixture containing a larger variety of polar and nonpolar model analytes. These included naphthalene, caffeine, pyrene, bisphenol A, inosine, cholesterol, and α -tocopherol. Large-area TENG MS successfully enabled the simultaneous detection of both protonated (Figure 3a) and low polarity (Figure 3b) species from these analytes. As expected, caffeine and inosine were also detected

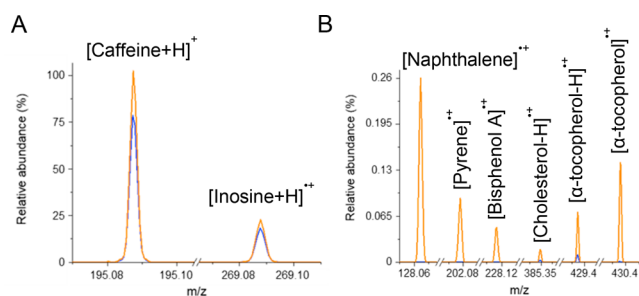


Figure 3. Large-area TENG (orange trace) and DC-nanoESI (blue trace) positive-ion mode analysis of a mixture containing both: (a) polar and (b) nonpolar compounds. The solution contained 20 μM of each naphthalene, caffeine, pyrene, bisphenol A, inosine, cholesterol, and α -tocopherol in a 1:1 water/methanol solution with 0.1%TFA. [Caffeine + H]⁺ was the base peak with an abundance of 1.07×10^8 .

with DC-nanoESI analysis, but only large-area TENG showed significant abundances for the $[\text{M}]^{\bullet+}$ ions of low polarity compounds. These ions were likely produced by gas-phase reactions in the corona discharge region between the emitter and the spectrometer inlet, therefore requiring molecular nitrogen or oxygen, as is typical of APCI. Modification of the TENG sprayer assembly to encapsulate the corona discharge region to decrease exposure to ambient air in the ionization region resulted in a sharp decrease in the abundances of such ions, confirming the likelihood that they were the product of gas-phase APCI processes (Figure S7).

To study the effectiveness of TENG in ionizing different polarity analytes in a more quantitative fashion, limits of

detection (LOD) for several of the model analytes tested above were determined (Figure S8 and Table S1), yielding excellent results. Parallel reaction monitoring (PRM) experiments for naphthalene yielded an LOD of 261 ppb while monitoring the m/z 102.05 fragment ion, whereas the LOD for inosine was 11.6 ppb for the m/z 135.03 ion and 6.1 ppb for the m/z 137.05 ion. These results confirmed the excellent sensitivity of TENG MS and suggested the possibility of using this technique for molecules of biological importance found in complex mixtures, as discussed below.

TENG Analysis of Unsaturated Lipids. During the experiments described in Figure 3, cholesterol and α -tocopherol oxidized species were readily observed (Figure S9), suggesting that gas-phase oxidation via TENG could potentially be leveraged to determine double bond position in unsaturated lipids via epoxidation.³⁴ Ozonolysis,^{35,36} high-energy collision-induced dissociation,³⁷ derivatization reactions,³⁸ ultraviolet photodissociation,³⁹ plasma oxidation,⁴⁰ and electrochemical epoxidation⁴¹ of double bonds have all been proposed as potential approaches to localizing double bonds. These approaches, however, typically require significant instrument modifications, use corrosive agents or specific reactants not always compatible with the various lipid classes, and may require time-consuming chemical reactions.

A model unsaturated FA, *cis*-vaccenic acid (VA), was chosen to investigate C=C location pinpointing using large-area TENG. The $[\text{VA} + \text{O} - \text{H}]^-$ ion at m/z 297.2 and $[\text{VA} + 2\text{O} - \text{H}]^-$ ion at m/z 313.2 (Figure 4a) were readily observed with a yield of approximately 11.9% and 8.3% when water/methanol 1:1 was used. This was found to be the optimum

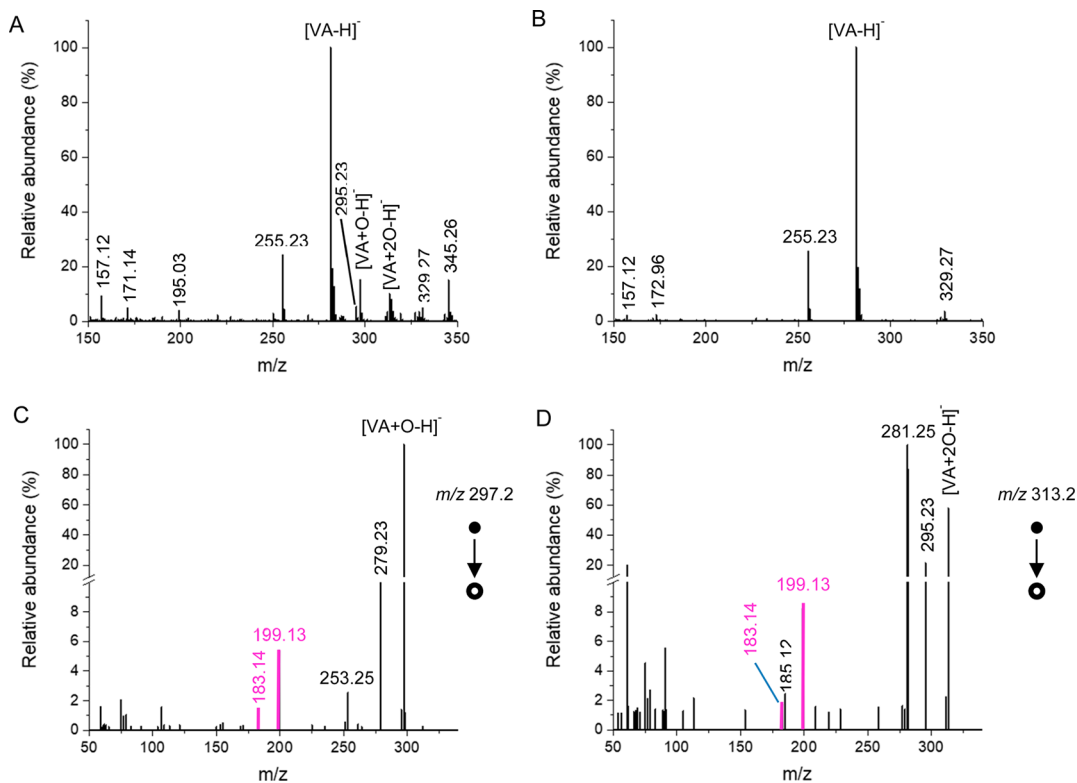


Figure 4. Mass spectrum of a 10 μM solution of *cis*-vaccenic acid (VA) ($\text{C}_{18}\text{H}_{34}\text{O}_2$) in water/methanol (1:1) with 50 mM NH_4OH analyzed via (a) large-area TENG and (b) DC nanoESI. Tandem MS experiments at a normalized collision energy of 35 for (c) the $m/z = 297.2$ $[\text{VA} + \text{O} - \text{H}]^-$ precursor ion, showing the m/z 183.1 and 199.1 diagnostic fragment ions and (d) the $m/z = 313.2$ $[\text{VA} + 2\text{O} - \text{H}]^-$ precursor ion, presenting similar fragments.

solvent in terms of spectral simplicity and overall sensitivity. Other solvents produced lower yields of the oxidized species, or more complex spectra, as discussed in Figure S10. Interestingly, the proportion of water in the solvent mixture was found to be important in terms of the extent of double bond oxidation (Figure S11). When the same solution was analyzed via DC-nanoESI at -1.5 kV, the epoxidation product was absent (Figure 4b). Tandem MS high-energy collision dissociation (HCD) experiments of the $[VA+O-H]^-$ ion resulted in two diagnostic fragments at m/z 183.1 and 199.1, characteristic of the unsaturation at the FA chain 11 position (Figure S12). Tandem MS of $[VA+2O-H]^-$ (m/z 313.2) showed that this oxidation product was also useful in pinpointing the C=C position (Figure 4d). Regardless of the precursor ion chosen, all these experiments demonstrated that large-area TENG enabled double bond localization in a rapid fashion and without the need for specific reagents.

The applicability of large-area TENG for C=C location pinpointing in lipids with a different C=C position (oleic acid, 9Z), and multiple unsaturations (linoleic acid, 9 and 12Z; α -linolenic acid, 9, 12 and 15Z) was also investigated. The observed epoxidation yield for oleic acid (OA) was similar to its structural isomer, *cis*-vaccenic acid (Figure S13a). Tandem MS analysis of $[OA+O-H]^-$ at $m/z = 297.2$ showed the two characteristic diagnostic peaks expected for the 9 position, m/z 155.11 and 171.1 (Figure S13d). This epoxide was accompanied by a secondary $[OA-2H+O-H]^-$ species at $m/z = 295.2$, which showed no interfering diagnostic peaks (Figure S13e). All other tested FAs also presented $[FA-2H+O-H]^-$ ions with similar behavior. Double bonds in multiply unsaturated FAs could also be localized using large-area TENG. As shown in Figure S13b,c, epoxidation of linoleic (LN) and linolenic (LNN) acids readily occurred, generating $[FA+O-H]^-$ and $[FA+2O-H]^-$ ions. Diagnostic fragment ions indicating the correct double bond positions (Figure S12) were obtained upon HCD of $m/z = 295.2$ ($[LN+O-H]^-$) and $m/z = 293.2$ ($[LNN+O-H]^-$), as shown in Figure S13f,g, respectively.

Following experiments with model FAs, analysis of a human serum sample was pursued to evaluate the applicability of large-area TENG MS to more complex samples. The protocol used for FA extraction from human serum is provided in the Supporting Information. As seen in Figure 5a, large-area TENG analysis of serum FA extract revealed the presence of various FAs (14:0, 14:1, 16:0, 16:1, 18:0, 18:1, 18:2 and 20:4), with the oxidation products for 18:1, 18:2, and 20:4 readily detected. For FA 14:1, the oxidation product was too weak, as the starting FA ion abundance was also low. The FA 16:1 oxidation product was confidently detected, but it was coselected with FA 17:0 in MS/MS experiments, so clean product ion spectra could not be obtained. Tandem MS experiments on the $[M+O-H]^-$ ion of FA 18:2 correctly localized the C=C at the 9 and 12 positions (Figure 5b). Similar experiments on the $[M+O-H]^-$ ion of FA 18:1 revealed a mixture of two different isobars, with the single double bond at position 9 or 11, the former in greater abundance (Figure 5c).

FA quantitation was performed using an isotopic dilution approach with spiked FA 17:0 as the internal standard. Good correlation was obtained between $[FA\ 18:1-H]^-$ ion abundance and its concentration (Figure S14a). Interestingly, good correlation was also observed for the $[FA\ 18:1+O-H]^-$ epoxidation product and concentration (Figure S14b),

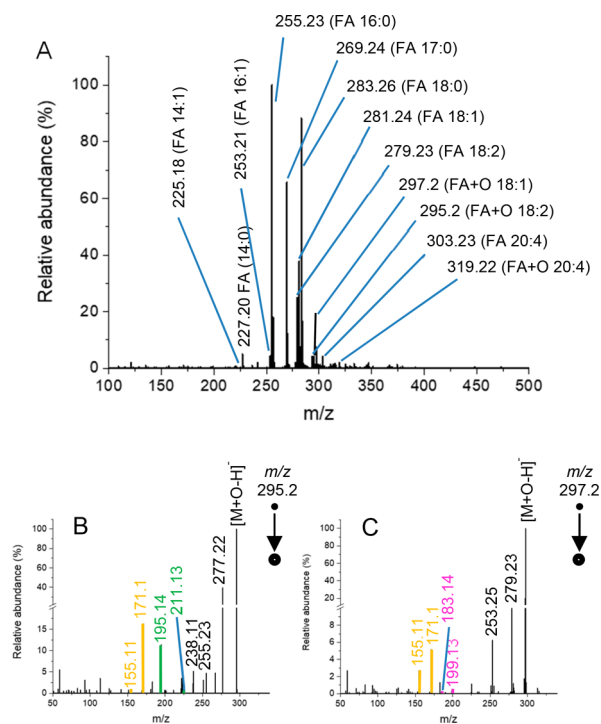


Figure 5. Large-area TENG MS analysis of a fatty acid (FA) extract from a human serum sample: (a) large-area TENG MS, (b) tandem MS of the 18:2 epoxide precursor ion (m/z 295.2), and (c) tandem MS of the 18:1 epoxide precursor ion (m/z 297.2).

suggesting this ionic species could also be used for quantitation purposes. As shown in Figure S14c, a calibration curve using the diagnostic fragment ion abundances for oleic and *cis*-vaccenic acid at molar ratios ranging from 1:1 to 1:15, allowed relative quantitation, finding the $\Delta 9$ and $\Delta 11$ isomers had 93.2% and 6.8% abundances.

Protein Analysis and Supercharging. Model proteins were also studied via large-area TENG to evaluate the influence of the increased number of delivered charges on the observed charge state distributions. Preliminary experiments with cytochrome C (Cyt C) solutions showed very good signal-to-noise ratios in both ion modes for all folded charge states observed, even at concentrations as low as 100 nM (Figure 6). Myoglobin TENG analysis also exhibited good sensitivity (Figure S15). Interestingly, it was observed that the high electric fields produced by large-area TENG promoted the formation of higher charge states for Cyt C, corresponding to unfolded structures (Figure 6a, inset). This effect was even more noticeable for myoglobin (Figure S15a). The unfolding and increase in average charge state (ACS) of myoglobin was clearly favored during large-area TENG operation in positive-ion mode, showing higher abundances for the apo form at charge states as high as +15 or +16. Detachment of the heme group was readily detected during TENG operation. We hypothesize that electrothermal supercharging, the shift in ACS to higher values without any reagents, first reported by Williams et al.,⁴² was responsible for the triboelectric-induced supercharging observed during these experiments.

Electrothermal supercharging represents an alternative means to induce protein ACS increases in native mass spectrometry and is a function of the voltage applied during the electrospray process, among other factors.⁴³ This phenomenon is the result of protein unfolding following

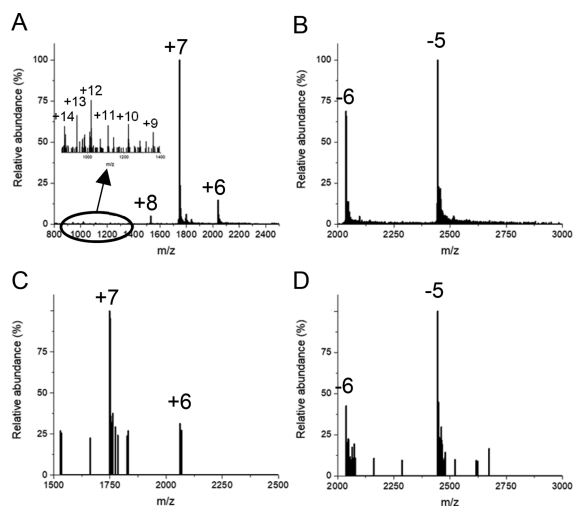


Figure 6. Large-area TENG analysis of different solutions of cytochrome C in water/methanol (1:1) + 100 mM of ammonium acetate: (a) 10 μM in positive-ion mode, (b) 100 nM in positive-ion mode, (c) 10 μM in negative-ion mode, and (d) 1 μM in negative-ion mode.

thermal denaturation induced by high electric fields.⁴⁴ While results shown in Figure 6a were obtained under denaturing conditions, native MS conditions were also tested with TENG MS. Under these conditions, both Cyt C and myoglobin showed a shift toward higher charge states that increased at shorter emitter-inlet distances, making unfolded ion structures more abundant (Figure 7). Reducing the area of the TENG

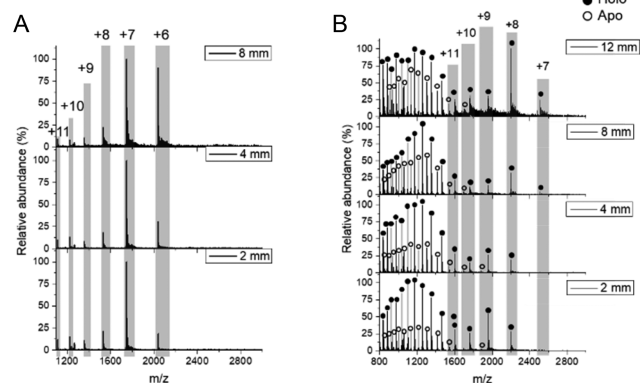


Figure 7. Control of protein charge states under electrothermal supercharging conditions using large-area TENG as a function of the nanoESI emitter-inlet distance to promote protein unfolding for (a) 10 μM cytochrome C in water with 100 mM NH_4Bic and (b) 10 μM myoglobin in water with 100 mM NH_4Bic .

slider electrode reduced the number of delivered charges and the open-circuit voltages, leading to the recovery of more folded +5 and +6 charge states (Figure S16).

CONCLUSIONS

In conclusion, large-area TENG have demonstrated significant enhancements to MS ion generation processes and are an interesting alternative to standard nanoESI power sources. Their charge delivery properties allows operation in a mixed regime that encompasses not only ESI, but also APCI, but without any detrimental effects to the emitters. This mixed regime enables ionization of challenging nonpolar compounds.

The higher pulsed voltages delivered by large-area TENG not only yielded high sensitivities, but also enabled maximum sample utilization efficiency by consuming only minute amounts (pL) of sample per pulse. Synchronization with mass analyzers such as ion traps, Orbitraps, and time-of-flight is possible for maximum ion utilization and duty cycle. Other TENG formats that allow high frequency switching, such as freestanding rotary devices,⁴⁵ could be useful in coupling this technology to liquid phase separations. Gas-phase oxidation at the nanoESI emitter was leveraged to induce epoxidation of lipid double bonds, which allowed pinpointing their position and their species-specific quantitation in biological samples. TENG ionization of proteins revealed excellent sensitivities and significant supercharging effects without the need for high surface tension additives, allowing to shift large molecular weight species to the m/z range where mass analyzers are at their best performance in terms of mass resolving power and accuracy, and producing multiply charged species that are more reactive precursors for tandem MS experiments.

ASSOCIATED CONTENT

Supporting Information

The Supporting Information is available free of charge at <https://pubs.acs.org/doi/10.1021/jasms.0c00002>.

Details on SF-TENG electrical characterization, reproducibility, automation, and pulsed mass spectrometry data interpretation, insights on the SF-TENG dual ionization mechanism, LODs, detailed information on fatty acids double bond pinpointing as well as protein analysis under native and non-native conditions (PDF)

AUTHOR INFORMATION

Corresponding Author

Facundo M. Fernández – School of Chemistry and Biochemistry, Georgia Institute of Technology, Atlanta, Georgia 30332, United States; NSF/NASA Center for Chemical Evolution, Atlanta, Georgia 30332, United States; orcid.org/0000-0002-0302-2534; Email: facundo.fernandez@chemistry.gatech.edu

Authors

Marcos Bouza – School of Chemistry and Biochemistry, Georgia Institute of Technology, Atlanta, Georgia 30332, United States; NSF/NASA Center for Chemical Evolution, Atlanta, Georgia 30332, United States

Yafeng Li – School of Chemistry and Biochemistry, Georgia Institute of Technology, Atlanta, Georgia 30332, United States

Changsheng Wu – School of Materials Science and Engineering, Georgia Institute of Technology, Atlanta, Georgia 30332, United States

Hengyu Guo – School of Materials Science and Engineering, Georgia Institute of Technology, Atlanta, Georgia 30332, United States

Zhong L. Wang – School of Materials Science and Engineering, Georgia Institute of Technology, Atlanta, Georgia 30332, United States; Beijing Institute of Nanoenergy and Nanosystems, Chinese Academy of Sciences, National Center for Nanoscience and Technology (NCNST), Beijing 100083, China

Complete contact information is available at: <https://pubs.acs.org/doi/10.1021/jasms.0c00002>

Author Contributions

All authors have given approval to the final version of the manuscript.

Notes

The authors declare no competing financial interest.

ACKNOWLEDGMENTS

This work was jointly supported by NSF and the NASA Astrobiology Program under the NSF Center for Chemical Evolution, CHE-1504217. We acknowledge Dr. Jean C. Rivera-Rios and Dr. Nga Lee Ng for assistance during DMA analysis.

REFERENCES

- (1) Yamashita, M.; Fenn, J. B. Electrospray ion source. Another variation on the free-jet theme. *J. Phys. Chem.* **1984**, *88*, 4451–4459.
- (2) Wilm, M.; Mann, M. Analytical Properties of the Nano-electrospray Ion Source. *Anal. Chem.* **1996**, *68*, 1–8.
- (3) Shen, Y.; Zhao, R.; Berger, S. J.; Anderson, G. A.; Rodriguez, N.; Smith, R. D. High-Efficiency Nanoscale Liquid Chromatography Coupled On-Line with Mass Spectrometry Using Nanoelectrospray Ionization for Proteomics. *Anal. Chem.* **2002**, *74*, 4235–4249.
- (4) Lu, W.; Bennett, B. D.; Rabinowitz, J. D. Analytical strategies for LC-MS-based targeted metabolomics. *J. Chromatogr. B: Anal. Technol. Biomed. Life Sci.* **2008**, *871*, 236–242.
- (5) Takáts, Z.; Wiseman, J. M.; Gologan, B.; Cooks, R. G. Mass Spectrometry Sampling Under Ambient Conditions with Desorption Electrospray Ionization. *Science* **2004**, *306*, 471.
- (6) Harris, G. A.; Galhena, A. S.; Fernández, F. M. Ambient Sampling/Ionization Mass Spectrometry: Applications and Current Trends. *Anal. Chem.* **2011**, *83*, 4508–4538.
- (7) Roach, P. J.; Laskin, J.; Laskin, A. Nanospray desorption electrospray ionization: an ambient method for liquid-extraction surface sampling in mass spectrometry. *Analyst* **2010**, *135*, 2233–2236.
- (8) Huang, G.; Li, G.; Cooks, R. G. Induced Nanoelectrospray Ionization for Matrix-Tolerant and High-Throughput Mass Spectrometry. *Angew. Chem., Int. Ed.* **2011**, *50*, 9907–9910.
- (9) Siegel, M. M.; Tabei, K.; Lambert, F.; Candelá, L.; Zoltan, B. Evaluation of a dual electrospray ionization/atmospheric pressure chemical ionization source at low flow rates (~50 $\mu\text{l}/\text{min}$) for the analysis of both highly and weakly polar compounds. *J. Am. Soc. Mass Spectrom.* **1998**, *9*, 1196–1203.
- (10) Cheng, S.-C.; Jhang, S.-S.; Huang, M.-Z.; Shiea, J. Simultaneous Detection of Polar and Nonpolar Compounds by Ambient Mass Spectrometry with a Dual Electrospray and Atmospheric Pressure Chemical Ionization Source. *Anal. Chem.* **2015**, *87*, 1743–1748.
- (11) Nemes, P.; Vertes, A. Laser Ablation Electrospray Ionization for Atmospheric Pressure, in Vivo, and Imaging Mass Spectrometry. *Anal. Chem.* **2007**, *79*, 8098–8106.
- (12) Özdemir, A.; Lin, J.-L.; Gillig, K. J.; Chen, C.-H. Kelvin spray ionization. *Analyst* **2013**, *138*, 6913–6923.
- (13) Qiao, L.; Sartor, R.; Gasilova, N.; Lu, Y.; Tobolkina, E.; Liu, B.; Girault, H. H. Electrostatic-Spray Ionization Mass Spectrometry. *Anal. Chem.* **2012**, *84*, 7422–7430.
- (14) Sweeting, L. M.; Cashel, M. L.; Rosenblatt, M. M. Triboluminescence spectra of organic crystals are sensitive to conditions of acquisition. *J. Lumin.* **1992**, *52*, 281–291.
- (15) Trimpin, S. “Magic” Ionization Mass Spectrometry. *J. Am. Soc. Mass Spectrom.* **2016**, *27*, 4–21.
- (16) Fan, F.-R.; Tian, Z.-Q.; Lin Wang, Z. Flexible triboelectric generator. *Nano Energy* **2012**, *1*, 328–334.
- (17) Wang, Z. L.; Lin, L.; Chen, J.; Niu, S.; Zi, Y. *Triboelectric Nanogenerators*; Springer International Publishing, 2016, 1–19.
- (18) Wang, Z. L. Triboelectric Nanogenerators as New Energy Technology for Self-Powered Systems and as Active Mechanical and Chemical Sensors. *ACS Nano* **2013**, *7*, 9533–9557.
- (19) Wang, Z. L.; Chen, J.; Lin, L. Progress in triboelectric nanogenerators as a new energy technology and self-powered sensors. *Energy Environ. Sci.* **2015**, *8*, 2250–2282.
- (20) Wang, S.; Lin, L.; Wang, Z. L. Triboelectric nanogenerators as self-powered active sensors. *Nano Energy* **2015**, *11*, 436–462.
- (21) Wang, S.; Zi, Y.; Zhou, Y. S.; Li, S.; Fan, F.; Lin, L.; Wang, Z. L. Molecular surface functionalization to enhance the power output of triboelectric nanogenerators. *J. Mater. Chem. A* **2016**, *4*, 3728–3734.
- (22) Li, A.; Zi, Y.; Guo, H.; Wang, Z. L.; Fernández, F. M. Triboelectric nanogenerators for sensitive nano-coulomb molecular mass spectrometry. *Nat. Nanotechnol.* **2017**, *12*, 481.
- (23) Bernier, M. C.; Li, A.; Winalski, L.; Zi, Y.; Li, Y.; Caillet, C.; Newton, P.; Wang, Z. L.; Fernández, F. M. Triboelectric nanogenerator (TENG) mass spectrometry of falsified antimalarials. *Rapid Commun. Mass Spectrom.* **2018**, *32*, 1585–1590.
- (24) Boys, B. L.; Kuprowski, M. C.; Noël, J. J.; Konermann, L. Protein Oxidative Modifications During Electrospray Ionization: Solution Phase Electrochemistry or Corona Discharge-Induced Radical Attack? *Anal. Chem.* **2009**, *81*, 4027–4034.
- (25) Kanev, I. L.; Mikheev, A. Y.; Shlyapnikova, Y. M.; Shlyapnikova, E. A.; Morozova, T. Y.; Morozov, V. N. Are Reactive Oxygen Species Generated in Electrospray at Low Currents? *Anal. Chem.* **2014**, *86*, 1511–1517.
- (26) Jaworek, A.; Sobczyk, A.; Czech, T.; Krupa, A. Corona discharge in electrospraying. *J. Electrostat.* **2014**, *72*, 166–178.
- (27) Tang, K.; Gomez, A. Generation of Monodisperse Water Droplets from Electrosprays in a Corona-Assisted Cone-Jet Mode. *J. Colloid Interface Sci.* **1995**, *175*, 326–332.
- (28) Borra, J. P.; Ehouarn, P.; Boulaud, D. Electrohydrodynamic atomisation of water stabilised by glow discharge—operating range and droplet properties. *J. Aerosol Sci.* **2004**, *35*, 1313–1332.
- (29) Ewing, R. G.; Waltman, M. J. Mechanisms for negative reactant ion formation in an atmospheric pressure corona discharge. *Int. J. Ion Mobility Spectrom.* **2009**, *12*, 65–72.
- (30) Morad, M. R.; Rajabi, A.; Razavi, M.; Sereshkeh, S. R. P. A Very Stable High Throughput Taylor Cone-jet in Electrohydrodynamics. *Sci. Rep.* **2016**, *6*, 38509.
- (31) Chen, D.-R.; Pui, D. Y. H.; Kaufman, S. L. Electrospraying of conducting liquids for monodisperse aerosol generation in the 4 nm to 1.8 μm diameter range. *J. Aerosol Sci.* **1995**, *26*, 963–977.
- (32) Hogan, C. J.; Kettleton, E. M.; Ramaswami, B.; Chen, D.-R.; Biswas, P. Charge Reduced Electrospray Size Spectrometry of Mega- and Gigadalton Complexes: Whole Viruses and Virus Fragments. *Anal. Chem.* **2006**, *78*, 844–852.
- (33) Davidson, K. L.; Oberreit, D. R.; Hogan, C. J.; Bush, M. F. Nonspecific aggregation in native electrokinetic nanoelectrospray ionization. *Int. J. Mass Spectrom.* **2017**, *420*, 35–42.
- (34) Zhang, J. I.; Tao, W. A.; Cooks, R. G. Facile Determination of Double Bond Position in Unsaturated Fatty Acids and Esters by Low Temperature Plasma Ionization Mass Spectrometry. *Anal. Chem.* **2011**, *83*, 4738–4744.
- (35) Brown, S. H. J.; Mitchell, T. W.; Blanksby, S. J. Analysis of unsaturated lipids by ozone-induced dissociation. *Biochim. Biophys. Acta, Mol. Cell Biol. Lipids* **2011**, *1811*, 807–817.
- (36) Harris, R. A.; May, J. C.; Stinson, C. A.; Xia, Y.; McLean, J. A. Determining Double Bond Position in Lipids Using Online Ozonolysis Coupled to Liquid Chromatography and Ion Mobility-Mass Spectrometry. *Anal. Chem.* **2018**, *90*, 1915–1924.
- (37) Tomer, K. B.; Crow, F. W.; Gross, M. L. Location of double-bond position in unsaturated fatty acids by negative ion MS/MS. *J. Am. Chem. Soc.* **1983**, *105*, 5487–5488.
- (38) Ma, X.; Xia, Y. Pinpointing Double Bonds in Lipids by Paternò-Büchi Reactions and Mass Spectrometry. *Angew. Chem., Int. Ed.* **2014**, *53*, 2592–2596.
- (39) Klein, D. R.; Brodbelt, J. S. Structural Characterization of Phosphatidylcholines Using 193 nm Ultraviolet Photodissociation Mass Spectrometry. *Anal. Chem.* **2017**, *89*, 1516–1522.
- (40) Zhao, Y.; Zhao, H.; Zhao, X.; Jia, J.; Ma, Q.; Zhang, S.; Zhang, X.; Chiba, H.; Hui, S.-P.; Ma, X. Identification and Quantitation of C-

C Location Isomers of Unsaturated Fatty Acids by Epoxidation Reaction and Tandem Mass Spectrometry. *Anal. Chem.* **2017**, *89*, 10270–10278.

(41) Tang, S.; Cheng, H.; Yan, X. On-Demand Electrochemical Epoxidation in Nano-Electrospray Ionization Mass Spectrometry to Locate Carbon-Carbon Double Bonds. *Angew. Chem., Int. Ed.* **2020**, *59*, 209.

(42) Sterling, H. J.; Cassou, C. A.; Susa, A. C.; Williams, E. R. Electrothermal Supercharging of Proteins in Native Electrospray Ionization. *Anal. Chem.* **2012**, *84*, 3795–3801.

(43) Mortensen, D. N.; Williams, E. R. Electrothermal supercharging of proteins in native MS: effects of protein isoelectric point, buffer, and nano ESI-emitter tip size. *Analyst* **2016**, *141*, 5598–5606.

(44) Zhao, F.; Matt, S. M.; Bu, J.; Rehrauer, O. G.; Ben-Amotz, D.; McLuckey, S. A. Joule Heating and Thermal Denaturation of Proteins in Nano-ESI Theta Tips. *J. Am. Soc. Mass Spectrom.* **2017**, *28*, 2001–2010.

(45) Cheng, J.; Ding, W.; Zi, Y.; Lu, Y.; Ji, L.; Liu, F.; Wu, C.; Wang, Z. L. Triboelectric microplasma powered by mechanical stimuli. *Nat. Commun.* **2018**, *9*, 3733.